A Generalised Lattice Boltzmann Equation on Unstructured Grids

Stefano Ubertini[1],[*]and Sauro Succi[2]

[1] *Università degli Studi di Roma, "Tor Vergata", Dip. Ingegneria Meccanica, Via del Politecnico, 1, 0133 Roma, Italia.*
[2] *Istituto Applicazioni del Calcolo CNR, Via del Policlinico, 137, 00161 Roma, Italia.*

Abstract. This paper presents a new finite-volume discretization of a generalised Lattice Boltzmann equation (LBE) on unstructured grids. This equation is the continuum LBE, with the addition of a second order time derivative term (memory), and is derived from a second-order differential form of the semi-discrete Boltzmann equation in its implicit form. The new scheme, named unstructured lattice Boltzmann equation with memory (ULBEM), can be advanced in time with a larger time-step than the previous unstructured LB formulations, and a theoretical demonstration of the improved stability is provided. Taylor vortex simulations show that the viscosity is the same as with standard ULBE and demonstrates that the new scheme improves both stability and accuracy. Model validation is also demonstrated by simulating backward-facing step flow at low and moderate Reynolds numbers, as well as by comparing the reattachment length of the recirculating eddy behind the step against experimental and numerical data available in literature.

1 Introduction

In the last decade, the lattice Boltzmann method (LBM) has become an established numerical approach in computational fluid dynamics. Many models and extensions have been formulated that cover a wide range of complex fluids and flows [1, 2]. The LBM, that originally evolved from lattice gas models, is based on a minimal kinetic Boltzmann

---

[*]Corresponding author. *Email addresses:* `stefano.ubertini@uniroma2.it` (S. Ubertini), `succi @iac.rm.cnr.it` (S. Succi)

equation in which representative particles ('parcels of fluids') evolve on a regular carte-
sian grid according to simple streaming and collide rules, designed in such a way as to
preserve the basic symmetries (conservation laws) of fluid dynamics. This method pos-
sesses some advantages over conventional CFD methods, such as the simplicity of the
stream-and-collide dynamics that makes LB very efficient from the computational point
of view, its amenability to parallel computing, its ease in handling complex flows and
the physical implementation of complex boundary conditions. However, the essential
restriction of the standard LBE to the lattice uniformity, which makes it macroscopically
similar to a uniform Cartesian-grid solver, represents a severe limitation for many practi-
cal engineering problems. Therefore, in the recent years, much research has been directed
to the goal of enhancing the geometrical flexibility of the LB method [3, 4, 15, 27].

Considering that for many practical problems an irregular grid or a meshless struc-
ture is always preferable due to the fact that curved boundaries can be described more
accurately, and that computational resources can be used more efficiently, our recent
effort is to extend the LBM order of accuracy and flexibility so that its spatial resolu-
tion requirements for various flow situations may be reduced and may be adapted to
more general meshes. Indeed, starting from the earliest finite-volume formulations more
than a decade ago [3], today many options are available to deal with realistically com-
plex geometries [5–8]. A particularly interesting development is represented by finite-
volume formulations on fully unstructured grids [9–11] which were recently extended
to 3D grids [12]. The Unstructured Lattice Boltzmann schemes (ULBE for short) inte-
grates the differential form of the Lattice Boltzmann equation (LBE) using a cell-vertex
finite-volume technique in which the unknown fields are placed at the nodes of the mesh
and evolve based on the fluxes crossing the surfaces of the corresponding control vol-
umes. These finite-volume formulations are best viewed as a coarse-grained version of
the original LB dynamics, in which geometrical flexibility is achieved at the level of the
coarse-graining elements, whose triangular (in two dimensions) or tetrahedral (in three
dimensions) shapes can accommodate the most complex geometries. Even if the ULBE
method is less efficient than the standard LBE in updating the single node, computational
savings are expected whenever the number of grid nodes can be reduced by, say, an or-
der of magnitude as compared to cartesian grids. Whether or not such a reduction can be
achieved depends of course on the geometrical complexity of the problem at hand, but
it is reasonable to expect that for highly complex geometries ULBE should indeed gain a
significant potential.

Nevertheless, the standard ULBE scheme suffers of the significant limitation $\Delta t < 2\tau$
which implies an adverse scaling of the time-step with the inverse Reynolds number
[11, 12]. In order to overcome the above mentioned stability limit a new scheme, called
ULBE with memory (ULBEM for short), has been developed [23] by introducing a 2nd or-
der term on the continuous lattice Boltzmann equation to be numerically solved through
a finite volume approach. This generalised formulation of the continuous lattice Boltz-
mann equation achieves better numerical stability and higher numerical accuracy, while
maintaining almost the same computational costs of the standard ULBE scheme. In this

paper, we give an analytical explanation of the new scheme advantages and we demonstrate the effectiveness of the ULBEM scheme against a laminar two-dimensional flow over a backward facing step for a Reynolds number up to 250.

2   Unstructured lattice Boltzmann equation

The ULBE scheme begins with the differential form of the single-time relaxation Lattice Boltzmann equation with particles velocity space properly discretized:

$$\partial_t f_i + \vec{c}_i \cdot \vec{\nabla} f_i = -(f_i - f_i^{eq})/\tau. \tag{2.1}$$

The above equation simulates transport phenomena by tracking the evolution of the density distribution function (or population) $f_i(\vec{x},t) \equiv f(\vec{x}, \vec{v} = \vec{c}_i, t)$, $i = 1, b$, that is a continuous function in physical space representing the probability of finding a particle at site $\vec{x}$, at time t moving along the lattice direction defined by the discrete speed $\vec{c}_i$. The left-hand side of this equation represents the molecular free-streaming, whereas the right-hand side represents molecular collisions via a single-time relaxation towards local equilibrium f_i^{eq} on a typical timescale τ [14]. The local equilibrium is the Maxwell-Boltzmann distribution function expanded in Taylor series of the fluid speed up to second order:

$$f_i^{eq} = \rho w_i [1 + \beta u_i + \frac{\beta^2}{2}(u_i^2 - u^2)], \tag{2.2}$$

where $\beta = 1/c_s^2$, being c_s the lattice sound speed, ρ the fluid density, $\vec{u}$ the fluid speed and w_i the associated weight coefficients. The macroscopic hydrodynamic quantities, such as fluid mass density and velocity, are obtained from the kinetic distribution by integration over velocity space: $\rho = \sum_i f_i$ and $\vec{u} = \sum_i \vec{c}_i f_i / \rho$. In the limit of weak departures from local equilibrium, i.e. small Knudsen numbers, it can be shown through a Chapman-Enskog analysis [1] that LBE recovers the dynamic behaviour of a fluid with pressure $P = \rho c_s^2$. In order to recover the correct fluid dynamic equations in the macroscopic limit, the set of discrete speeds must satisfy mass, momentum and energy conservation, as well as rotational symmetry. It should be noted that only a limited class of lattices exhibits the right symmetry to ensure the conservation constraints. In the present work we shall refer to the two-dimensional nine-speed model (known as D2Q9) defined by the following set of discrete speeds [14]:

$$c_i = \begin{cases} 0, & i = 0, \\ \cos((i-1)\pi/2), & i = 1, \cdots, 4, \\ \sqrt{2}\cos(\pi/4 + (i-5)\pi/2), & i = 5, \cdots, 8, \end{cases} \tag{2.3}$$

with weights $w_0 = 4/9$, $w_1 = 1/9$, $w_2 = 1/36$ in Eq. (2.2). The ULBE approach to numerically solve Eq. (2.1) is a finite-volume scheme of the cell-vertex type by introducing a tessellation based on triangular elements. The use of unstructured grids with control volumes of arbitrary polyhedral shape allows local grid refinements not possible with
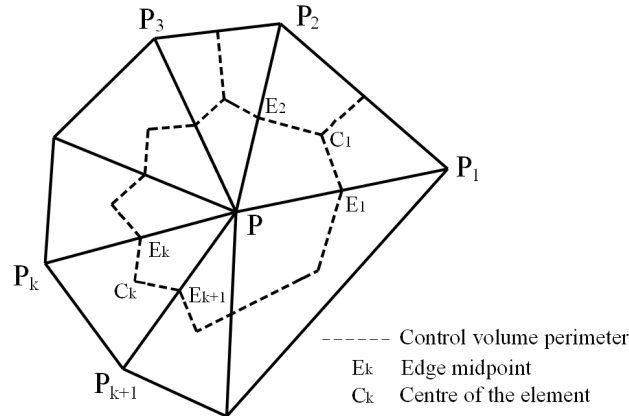
Figure 1: Geometrical layout of the cell-vertex finite volume discretization around a grid point P.

the standard BGK. The nine discrete populations $f_i(\vec{x},t)$ associated to each node P of the discrete grid (Fig. 1) represent the unknowns of the problem. The finite volume over which Eq. (2.1) is integrated is defined by means of the set of K triangles, which share P as a common vertex. Since the discrete grid is unstructured, each node is identified by its coordinates and the connectivity (P, P_k, P_k+1 in Fig. 1) is free to change from node to node. As shown in Fig. 1, the portion of the control volume $[C_k,E_k,P,E_k+1]$ that refers to the k-th triangular element is built through the union of the two sub-grid triangles $\Omega_k^- = [P,E_k,C_k]$ and $\Omega_k^+ = [P,C_k,E_{k+1}]$, where C_k is the centre of the grid element and E_k and E_k+1 are the midpoints of the edges that share P as a common vertex. Populations at off-grid points E_k and C_k are calculated with standard linear interpolations. Application of the Gauss theorem to each finite volume portion yields the following set of ordinary differential equations:

$$\partial_t f_i(P,t) = \frac{1}{V_P}\sum_k (\Phi_{ik}-\Xi_{ik}),\qquad(2.4)$$

where the sum $k=0,K$ runs over the control volume $\Omega_P = \cup_k \Omega_k$ obtained by joining the centres C_k with edge midpoints E_k, V_P is the magnitude of the control volume around P and the index $k=0$ denotes the pivotal point P. Finally, Φ_{ik} denote the fluxes associated with the streaming operator and Ξ_{ik} the integral of the collision operators of the i-th population at the k-th node, respectively. The detailed expressions of the streaming and collision matrices S_{ik} and $C_{ik}=C_k\delta_{ik}$, give the following general form of the Unstructured Lattice Boltzmann Equation (ULBE):

$$\partial_t f_i(P,t) = \sum_{k=0}^{K} S_{ik} f_i(P_k,t) - \frac{1}{\tau}\sum_{k=0}^{K} C_{ik}[f_i(P_k,t)-f_i^{eq}(P_k,t)].\qquad(2.5)$$

By definition the following sum rules apply:

$$\sum_{k=0}^{K} S_{ik}=0, \quad \sum_{k=0}^{K} C_{ik}=1, \quad \forall i.$$

3   ULBE with memory scheme

In the original LB scheme the space-time discretization of the differential equation (2.1) is performed through an explicit finite differencing along the particle trajectories (straight lines since the discrete speeds are constant). Considering a second-order strategy for the time finite differencing, the lattice Boltzmann equation with BGK approximation reads as follows:

$$f_i(\vec{x}+\vec{c}_i\delta t,t+\delta t)=f_i(\vec{x},t)-\frac{\delta t}{2\tau}[(f_i(\vec{x},t)-f_i^{eq}(\vec{x},t))+(f_i(\vec{x},t+\delta t)-f_i^{eq}(\vec{x},t+\delta t))]. \quad (3.1)$$

By making the following variable change [17]:

$$f_i^*=f_i-\frac{\delta t}{2\tau}(f_i-f_i^{eq}), \quad (3.2)$$

the following explicit evolution equation for f_i^* is obtained:

$$f_i^*(\vec{x}+\vec{c}_i\delta t,t+\delta t)=f_i^*(\vec{x},t)-\frac{\delta t}{\tau+\frac{1}{2}\delta t}(f_i^*(\vec{x},t)-f_i^{eq}(\vec{x},t)). \quad (3.3)$$

The nice property gained with the above substitution is that the basic hydrodynamic quantities can be still obtained through simple moment summations of the f_i^*:

$$\rho=\sum_i f_i=\sum_i f_i^*, \quad (3.4)$$

$$\vec{u}=\sum_i \vec{c}_i f_i/\rho=\sum_i \vec{c}_i f_i^*/\rho, \quad (3.5)$$

thus avoiding the necessity to solve the implicit Eq. (3.1). A continuous form of Eq. (3.1) can be obtained through a 2nd order Taylor-series expansion in the least-squares-based form:

$$\partial_t f_i^*+\vec{c}_i\cdot\vec{\nabla} f_i^*+\frac{1}{2}\delta t\partial_{tt} f_i^*+\frac{1}{2}\vec{c}_i\vec{c}_i\delta t:\vec{\nabla}\vec{\nabla} f_i^*=-\frac{1}{\tau+\frac{1}{2}\delta t}(f_i^*-f_i^{eq}). \quad (3.6)$$

This has the form of a generalized (time-delayed) Boltzmann equation, discussed in depth by Alexeev [26], with the identification of his collision time with $-\delta t/2$. It should be noted that the negative sign (anticipation) corresponds to negative diffusion and is directly related to the so-called propagation viscosity. Therefore, at variance with Alexeev, the additional term $\delta t/2$ in the collision operator lets ULBEM recover the same viscosity as in the continuum $\nu=c_s^2\tau$.

Grouping $\partial_t+\vec{c}_i\cdot\vec{\nabla}$ in the operator D_i, Eq. (3.6) can be written as:

$$D_i f_i^*+\frac{\delta t}{2}D_i^2 f_i^*=-\frac{1}{\tau+\frac{1}{2}\delta t}(f_i^*-f_i^{eq}). \quad (3.7)$$

This equation, a close analogue of telegrapher's equation, can be assimilated to the continuous LBE with the addition of a 2nd order term $\frac{\delta t}{2}D_i^2 f_i^*$, from now on called memory term.

After one has obtained (3.4), it is not necessary to come back again to the continuous equation (3.7) to perform discretization in space (3.11)-(3.12). In fact, as was shown in [18], Eq. (3.4) is already sufficient to do finite elements or finite difference discretization directly on (3.4), which overcomes the CFL limitation of (3.1), same as done here.

By making the substitution $g_i = D_i$, the first-order form of Eq. (3.7) is obtained and the mathematical model is reduced to the following system of two first-order differential equations:

$$D_i f_i^* = g_i, \tag{3.8}$$

$$D_i(f_i^* + \frac{\delta t}{2}g_i) = -\frac{1}{\tau + \frac{1}{2}\delta t}(f_i^* - f_i^{eq}), \tag{3.9}$$

that can be numerically solved through the cell-vertex finite-volume technique. In terms of the streaming and collision matrices in Eq. (2.5), the time-marching solution proceeds according to the following sequence of equations:

$$g_i(P,t+\Delta t) = -g_i(P,t) + \Delta t \sum_{k=0}^{K} S_{ik}g_i(P_k,t) - \frac{2}{\tau + \frac{\Delta t}{2}}\sum_{k=0}^{K}C_{ik}[f_i^*(P_k,t) - f_i^{eq}(P_k,t)], \tag{3.10}$$

$$f_i^*(P,t+\Delta t) = f_i^*(P,t) + \Delta t \sum_{k=0}^{K} S_{ik}f_i^*(P_k,t) + [g_i(P,t+\Delta t) + g_i(P,t)]\frac{\Delta t}{2}, \tag{3.11}$$

called from now on *ULBE with Memory* (*ULBEM* for short). It is important to note that the system can be solved in one iteration, since the updated solution of the g function, $g_i(P,t+\Delta t)$, needed in the second equation, is explicitly calculated from the first one.

The covolume boundary condition treatment already developed for the standard ULBE [10] can be easily extended to ULBEM. In the covolume method, the fluxes across boundary edges are evaluated by explicit interpolation. For non-slip boundary conditions, the equilibrium populations at the boundary nodes are computed as local equilibria with the wall speed $\vec{u} = \vec{u_W}$. For open boundaries the equilibria are obtained by imposing the desired density at the outlet and velocity at the inlet and importing the velocity at the outlet and the density at the inlet from the closest interior nodes. In this procedure, the computational domain is augmented with one (or more) buffers of uniform triangles. The scope of these regular buffers is to ensure that the last-but-one row of nodes faces with a corresponding neighbor along the streamwise direction, so that, by imposing the same value on these two rows of nodes, a zero-longitudinal-gradient boundary condition is automatically fulfilled.

In actual implementations, the extra cost of memory and gradient calculation in the ULBE with memory scheme for each time step is minor with respect to the standard ULBE. In fact, the real cost comes from the additional step for the calculation of the g

function and the additional memory for storing the g values, while the streaming and collision matrices remain unchanged. The time required for each iteration is increased of less than 10 percent, but the total simulation time is significantly reduced by the increased time-step.

4   Stability constraints

The kinematic viscosity of the ULBE scheme was found [10, 12] to be $\nu = c_s^2 \tau$, like in the continuum. This contrasts with standard LB, which features $\nu = c_s^2(\tau - \Delta t/2)$. The shift $-\Delta t/2$ has far-reaching consequences for the computational efficiency of high-Reynolds number flow simulations. To appreciate the point, let us remind that, due to the explicit time-integration of the collision term, both LB and ULBE are subject to the CFL (Courant-Friedrichs-Lewy) stability constraint:

$$\Delta t < 2\tau. \tag{4.1}$$

Since the ULBE viscosity is proportional to the relaxation time, vanishingly low viscosities imply a correspondingly vanishingly low τ. Due to the stability constraint (4.1), this leads to a collapse of the timestep for high-Reynolds flow simulations. Thanks to the negative shift $-\Delta t/2$, standard LB is free from such limitation, because vanishingly small viscosities $\nu = \mathcal{O}(\epsilon)$ can be achieved with finite timestep $\Delta t = 2\tau - \epsilon$. This shift is peculiar to LB schemes in uniform lattices, in which space and time are linked up by the light-cone condition $\Delta x = c\Delta t$, and consequently for generic grid settings, the only possibility to avoid the aforementioned timestep collapse is to find ways out of the CFL stability constraint. In this work, a new version of ULBE is presented which proves capable of achieving this goal.

It is worth expanding the discussion of time-marching schemes in some more detail. Consider the linear kinetic equation $df/dt = -f/\tau$, where all indices are removed for the sake of simplicity, and integrate it in time with a first-order Euler forward scheme. This yields:

$$f(t+\Delta t) - f(t) = -\frac{\Delta t}{\tau} f(t). \tag{4.2}$$

The CFL stability condition imposes $|1 - \Delta t/\tau| < 1$, that is $0 < \Delta t < 2\tau$. Next, consider the following second-order kinetic equation:

$$m\frac{d^2 f}{dt^2} + \frac{df}{dt} = -\frac{f}{\tau}, \tag{4.3}$$

where we have added a second-order inertial (memory) term driven by the parameter m. It is readily shown that a time-centered scheme leads *exactly* to the same first-order discrete equation (4.2), provided the coefficient $m = \Delta t/2$. This shows that, in spite of its first-order appearance, the discrete scheme (4.2) is a second-order discretization of the second-order continuum kinetic equation. Clearly, this is only true if $m = \Delta t/2$. Upon turning

the time-derivative df/dt into a full streaming operator $Df \equiv \partial_t f + v\partial_x f$, the above discretization delivers precisely the standard LB scheme. The presence of the second-order derivative implies i) second-order time-accuracy, ii) the shift in the kinematic viscosity $\nu = c_s^2(\tau - \Delta t/2)$. This expression shows that the CFL range of stability coincides exactly with the positivity domain of the kinematic viscosity. The negative shift $-\Delta t/2$, known as 'propagation viscosity', stems from second order terms of the Taylor expansion of the discrete streaming operator, as required to correctly recover the diffusive stage of the hydrodynamic equations. As previously mentioned, this very favourable situation dissolves as soon as the space and time discretizations are divorced from the lightcone condition. Away from this special situation, one is forced to seek for time-marching schemes capable of overcoming the CFL constraints. A natural move in this direction is to resort to *locally implicit* formulations, of the form [17,18]:

$$f(t+\Delta t) - f(t) = -\frac{\Delta t}{\tau} \frac{f(t) + f(t+\Delta t)}{2}. \tag{4.4}$$

This introduces a non-causal dependency between the right and left hand side, which removes the CFL stability constraint. Indeed, it is a simple matter to show that the propagator from time t do $t+\Delta t/2$ takes now the form:

$$P_{\Delta t} = \frac{1 + \Delta t/2\tau}{1 - \Delta t/2\tau}$$

so that the stability condition $|P| < 1$ is unconditionally fulfilled for any value of the time-step. Normally, implicit time-stepping introduces global space-dependencies which give rise to expensive matrix problems. However, thanks to the local structure of the collision operator (a diagonal matrix in the especially simple case of BGK), the linear equation above can be inverted site-by-site on purely algebraic means. This is the basic reason why the implicit formulation can still be recast in simple explicit form. Indeed, simple algebra shows that (4.4) is strictly equivalent to an Euler-forward time marching scheme for the rescaled distribution $\tilde{f} = (1 - \Delta t/2\tau)f$, with a rescaled relaxation frequency $\tilde{\omega} = \omega/(1+\Delta t/2\tau)$. The corresponding viscosity is then turned into

$$\tilde{\nu} = c_s^2(\tau(1+\Delta t/2\tau) - \Delta t/2) = c_s^2\tau$$

indicating that the propagation viscosity is reabsorbed away, thus leading to the same expression as in the continuum. The change in (computational) perspective emerges quite neatly. To achieve viscosities $\mathcal{O}(\epsilon)$, the relaxation time τ must be order ϵ too. However, since the CFL constraint no longer applies, one is free to choose $\Delta t > 2\tau$. In particular, to be competitive with the explicit scheme, one needs to make $\Delta t \sim \tau/\epsilon$. This is certainly advantageous for high-viscous flows, where $\epsilon \sim 1$, but raises a serious challenge when $\epsilon < 0.01 - 0.001$, as in standard LB practice for high-Reynolds flow simulations. To date, ULBE implementations based on the locally implicit scheme have proven capable of producing competitive results up to $dt \sim 10\tau$. At the current levels of spatial resolution, this

is not sufficient to make them competitive with standard LB for values of the Reynolds number above a few hundreds. ULBE versions with memory term have been recently shown to bring sensible benefits in this direction. Again, a few detailed remarks are in order. Let us consider again the second-order kinetic equation $df/dt + \frac{dt}{2}d^2f/dt^2 = -f/\tau_r$, where we have defined the effective relaxation time as $\tau_r = \tau + \Delta t/2$. To the purpose of time-integration, the above equation is best recast in the form of two first-order equations, in analogy with Hamiltonian dynamics:

$$\dot{f} = g, \tag{4.5}$$

$$g + \frac{\Delta t}{2}\dot{g} = -f/\tau_r, \tag{4.6}$$

where $\dot{f}, \dot{g}$ mean time derivatives. Euler integration of the second equation delivers:

$$\frac{g + g(t+\Delta t)}{2} = -\frac{\Delta t}{\tau_r}f. \tag{4.7}$$

The simultaneous dependence introduced by $g(t+\Delta t)$ can be disposed of by advancing the second equation with a mid-point rule:

$$f(t+\Delta t) - f(t) = \frac{\Delta t}{2}(g(t) + g(t+\Delta t)). \tag{4.8}$$

Combination of the two expressions above delivers

$$f(t+\Delta t) = (1 - \frac{\Delta t}{\tau_r})f(t), \tag{4.9}$$

which retains the formal structure of an explicit Euler-forward scheme, with an effective relaxation time τ_r, hence a kinematic viscosity $\nu = c_s^2\tau$. Being based on implicit time-marching, the scheme is second-order time accurate. On the other hand, due to the very definition of τ_r, the CFL condition associated with (4.9), i.e $|1 - \Delta t/\tau_r|$, is unconditionally fulfilled. This proves that the present scheme achieves both second-order accuracy and unconditional stability, while still retaining the simple structure of an explicit Euler time-marching. These remarkable properties stem from the combination of three basic ingredients:

   i. Start from a second-order kinetic equation in the continuum;

  ii. Locally implicit time-marching discretization;

 iii. Use of a rescaled relaxation time $\tau_r = \tau + \Delta t/2$.

Key to the success of this program is the structure of kinetic equations, which permits to turn implicit relations into explicit ones by elementary local algebraic inversion. For the especially simple case of single-time (diagonal) collision operators, this local inversion amounts to an elementary rescaling of the relaxation time.
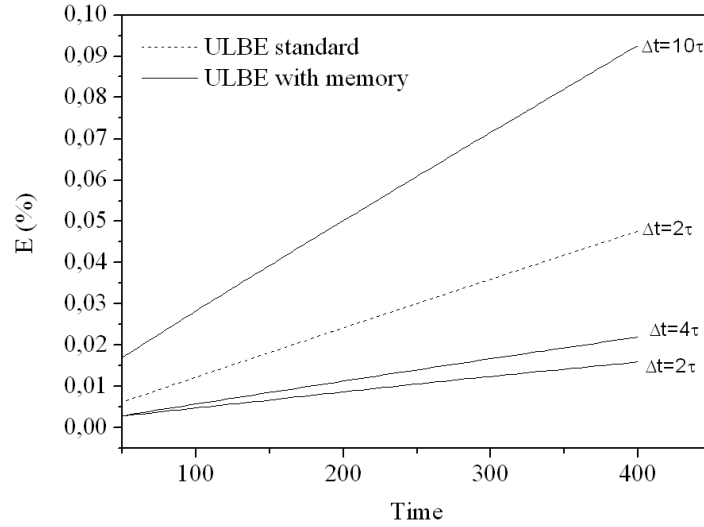
Figure 2: Relative velocity error.

5 Numerical results

5.1 Taylor-vortex flow

The effective viscosity of the method has been measured by setting up a freely decaying two-dimensional Taylor-vortex flow in a box of size W. Comparing the numerical results with the analytical solution [23] the same viscosity of the standard ULBE, $\nu = c_s^2 \tau$, is determined. However, while the standard ULBE could perform simulations with time steps only up to 2τ, using the ULBE with memory scheme in a box of 2145 triangular elements the time step could be raised up to $\Delta t = 40\tau$ as shown in a previous paper [23]. This gives a clear indication that the constraint $\Delta t < 2\tau$ is overcome by the ULBE with memory method and that the time step limit is set by the local Courant number, as for traditional CFD methods. Defining the relative velocity error variation as follows:

$$E = \frac{\sum_{x,y}(|u_1 - u_0| + |v_1 - v_0|)}{\sum_{x,y}(|u_0| + |v_0|)} \tag{5.1}$$

being u and v the x- and y-component of velocity, respectively, and the subscripts 0 and 1 the analytical and the numerical result, respectively, Fig. 2 compares the accuracy of the new scheme with the standard ULBE for a Taylor vortex flow simulation with a first-order explicit time-stepping scheme has been used. It can be observed that with the same Δt the ULBE with memory is much more accurate than standard ULBE. Moreover, for $\Delta t = 4\tau$, the error E is even lower than that for $\Delta t = 2\tau$. This can be explained by considering that there are two main sources of error: a systematic error, which is related to the fact that the solid boundary is not exactly placed at the boundary nodes and the temporal
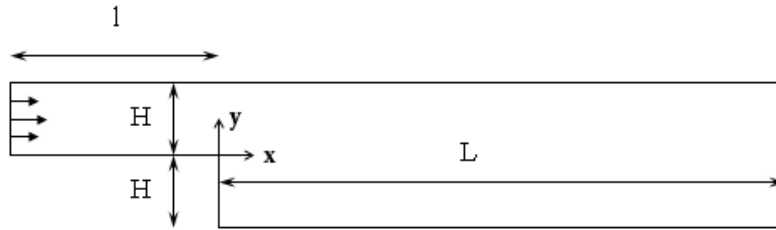
Figure 3: Geometry of the backward facing step.

discretization error. The first one increases with the number of iterations and then is reduced by increasing the time step. The latter is obviously proportional to the time-step length. It is worth noting that the relative error is still very low even for $\Delta t = 10\tau$.

5.2 Backward facing step

In this section the ULBE with memory scheme is tested against a laminar flow over a backward facing step, which is one of the most fundamental forms of flow separation in fluid mechanics and has been extensively studied both numerically and experimentally [19–22, 24, 25]. This test is an established and hard benchmark test in computational fluid dynamics as the resulting recirculating flow region is highly skewed with respect to the numerical mesh and its characteristics are difficult to be predicted as even a low numerical diffusion may significantly affect them.

The study is performed on the step channel configuration originally considered by Armaly et al. [19] and shown in Fig. 3. The fluid is assumed to have constant density and constant kinematic viscosity and the flow moves toward the larger gap (i.e., a backward-facing step). The backward facing step has a nominal expansion ratio of 2. Being H the height of the inlet duct, the entrance channel length is $l = 4.5H$, thus preventing downstream effects of the inlet boundary conditions. The outlet channel is truncated at $L = 10.5H$ in order to avoid any alteration of the flow region behind the step. The simulation at $Re = 20$, 50 and 100 have been performed on a mesh with 3010 nodes and 5722 elements. For $Re > 100$ the computational grid has been refined up to 6300 nodes and 12410 elements (see Fig. 4) with local grid refinement around the step corners and behind the step where the vortex formation is predictable.

The flow has been numerically simulated for Reynolds number ranging between 20 and 250, being the Reynolds number defined as follows:

$$Re = \frac{2\rho U_M H}{\nu}, \tag{5.2}$$

where U_M is the maximum speed at inlet. The flow is initially at rest (zero speed) and is impulsively started by forcing a parabolic profile at inlet. The chosen outflow boundary
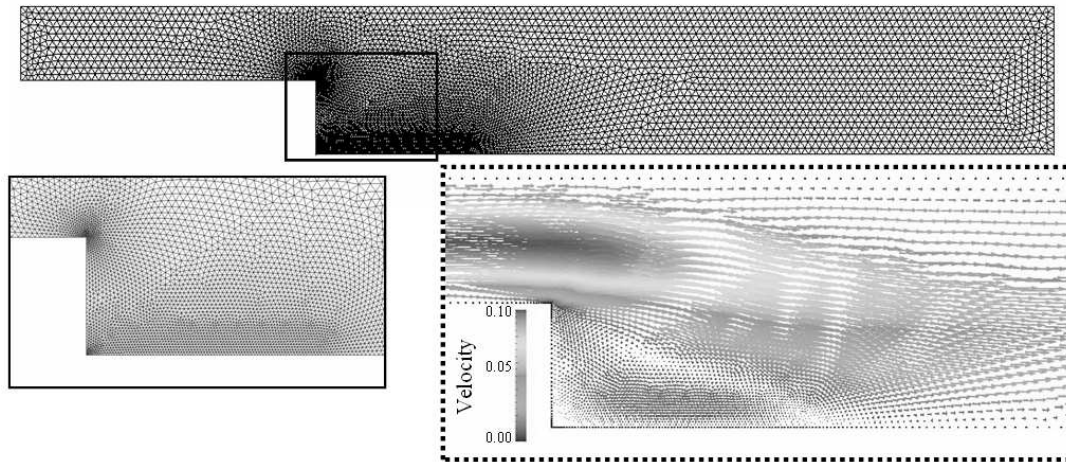
Figure 4: Numerical mesh and detail of the flow field behind the step at Re=100.

condition is the zero-longitudinal velocity gradient. Along the solid boundaries the non-slip boundary condition through the covolume method is applied. In all the simulations the facing step height and the free stream velocity (Mach number) were kept constant and the various Reynolds numbers were thus obtained by changing the relaxation parameter.

Fig. 5 shows the contour of the stream function inside the channel for two values of Re (100 and 150) in terms of streamlines and velocity distribution. Even if the geometry of the channel is simple, the flow pattern is fairly complex. As the flow reaches the enlargement, the flow velocity suddenly drops, the pressure rises and the flow separates at the step corner. This flow separation is followed by a region of recirculating fluid behind the step. The outlet channel is long enough to allow the flow developing into a fully developed profile. The detail of the flow field behind the step that could be obtained through the unstructured grid can be observed in Fig. 4. Below Reynolds number 200 the flow is essentially steady and span wise invariant with a stable primary eddy behind the step.

As the Reynolds number increases, the eddy behind the step becomes larger and the point of flow reattachment moves toward the outlet section. The location of the flow reattachment point, that is the length of the recirculating flow downstream of the step, is often taken as a measure of the predictive capability and the computational accuracy of a CFD code. It mainly depends on the channel geometry (width ratio before and after the step) and the Reynolds number. The predicted reattachment distance from the step as a function of the inlet Reynolds number is shown and compared to data found in literature [19–22, 24, 25] in Fig. 6. The flow reattachment point is defined by a change in sign of the vorticity. The observed excellent agreement with literature data indicates that the ULBE with memory scheme is at the same time at least as accurate as the original ULBE at the same resolution for low *Re* and gains stability as it allows simulating the
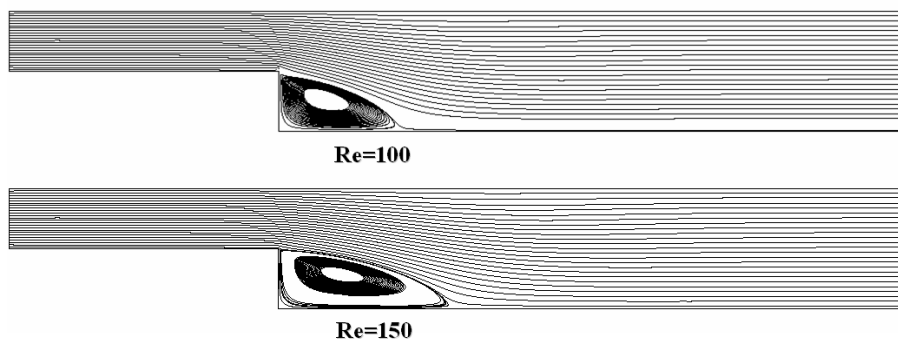
Figure 5: Streamlines showing the flow structures at different Reynolds numbers.
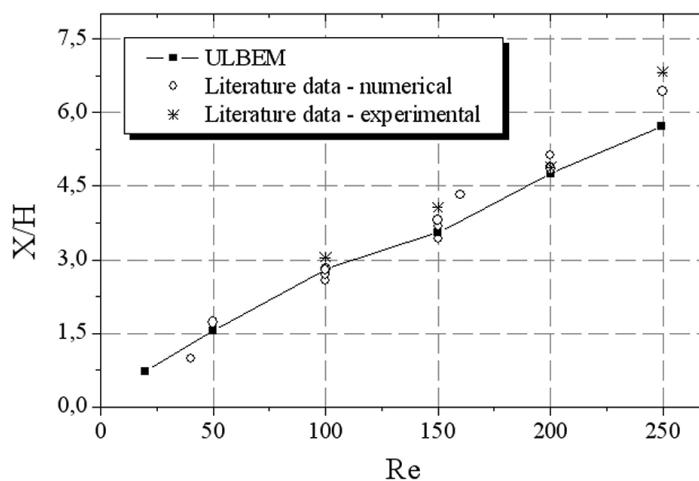
Figure 6: Reattachment lengths in function of the Reynolds number: comparison with literature data [19–22, 24, 25].

flow at higher Reynolds with minor time steps. Poor agreement is observed only for *Re*=250 when the flow unsteadiness begins to be significant, as the expansion flow along the outlet channel has the tendency to form a new separation zone.

6 Conclusions

A new form of Lattice Boltzmann equation on unstructured grids is derived by applying implicit time-marching discretization to a continuum Boltzmann equation with second-order memory term. The new model has been tested against the Taylor vortex flow and the flow past a backward facing step and an excellent agreement with literature results from incompressible codes and experiments is observed. The main feature of the new

approach is that the ULBE stability constraint $\Delta t < 2\tau$ no longer applies. The numerical results show that, as compared with the standard ULBE, the new model:

- is more accurate;
- the stability constraint $\Delta t < 2\tau$ is lifted;
- it can be advanced in time with much larger time-steps than previous unstructured LB schemes;
- is more stable.

On the other hand, further improvements are still necessary in order to gain further stability and extend the simulation to higher Reynolds numbers unsteady flows. Work along these lines is in progress.

References

[1] R. Benzi, S. Succi and M. Vergassola, The lattice Boltzmann equation: theory and applications, Phys. Rep., 222 (1992), 145.
[2] D. A. Wolf-Gladrow, Lattice-Gas Cellular Automata and Lattice Boltzmann Models: An Introduction, Springer, 2000.
[3] F. Nannelli and S. Succi, The lattice Boltzmann equation in irregular lattices, J. Stat. Phys., 68 (1992), 401.
[4] H. Chen, Volumetric formulation of the lattice Boltzmann method for fluid dynamics: basic concept, Phys. Rev. E, 58 (1998), 3955.
[5] N. Cao, S. Chen, S. Jin and D. Martinez, Physical symmetry and lattice symmetry in the lattice Boltzmann method, Phys. Rev. E, 55 (1997), R21.
[6] X. He, L. Luo and M. Dembo, Some progress in lattice Boltzmann method. Part I. Nonuniform mesh grids, J. Comput. Phys., 129 (1996), 357.
[7] O. Filippova and D. Hanel, Grid refinement for lattice-BGK models, J. Comput. Phys., 147 (1998), 219.
[8] I. V. Karlin, S. Succi and S. Orszag, Lattice Boltzmann method for irregular grids, Phys. Rev. Lett., 82 (1999), 5245.
[9] G. Peng, H. Xi and C. Duncan, Lattice Boltzmann method on irregular meshes, Phys. Rev. E, 58 (1998), R4124.
[10] S. Ubertini, G. Bella and S. Succi, Unstructured lattice Boltzmann method: further developments, Phys. Rev. E, 68 (2002), 016701.
[11] S. Ubertini, S. Succi and G. Bella, Lattice Boltzmann schemes without coordinates, Philos. T. Roy. Soc. A, 362(1821) (2004), 1763.
[12] N. Rossi, S. Ubertini, G. Bella and S. Succi, Unstructured lattice Boltzmann method in three dimensions, Int. J. Numer. Meth. Fluids, 49(6) (2005), 619.
[13] R. Mei, D. Yu, W. Shyy and L.-S. Luo, Force evaluation in the lattice Boltzmann method involving curved geometry, Phys. Rev. E, 65(4) (2002), 041203.
[14] Y. Qian, D. d'Humieres and P. Lallemand, Lattice BGK models for Navier-Stokes equation, Europhys. Lett., 17 (1992), 479.
[15] R. Mei, L.-S. Luo and W. Shyy, An accurate curved boundary treatment in the lattice Boltzmann method, J. Comput. Phys., 155 (1999), 307.
[16] S. Ubertini and S. Succi, Recent advances of lattice Boltzmann techniques on unstructured grids, Prog. Comput. Fluid Dyn., 5(1/2) (2005), 85.

[17] X. He, S. Chen and G. D. Doolen, A novel thermal model for the lattice Boltzmann method in incompressible limit, J. Comput. Phys., 146 (1998), 282.

[18] A. Bardow, I. V. Karlin and A. A. Gusev, General characteristic-based algorithm for off-lattice Boltzmann simulations, Europhys. Lett., 75 (2006), 434.

[19] F. Armaly, F. Durst, J. C. F. Pereira and B. Schonung, Experimental and theoretical investigation of backward facing step flow, J. Fluid Mech., 127 (1983), 473.

[20] L. Kaiktis, G. E. Karniadakis and S. A. Orzag, Onset of three-dimensionality, equilibria, and early transition in flow over a backward facing step, J. Fluid Mech., 231 (1991), 501.

[21] J. Kim and P. Moin, Application of a fractional-step method to incompressible Navier-Stokes equation, J. Comput. Phys., 59 (1985), 308.

[22] I. E. Barton, Computation of particle tracks over a backward-facing step, J. Aerosol Sci., 26(6) (1995), 887.

[23] S. Ubertini, G. Bella and S. Succi, Unstructured lattice Boltzmann equation with memory, Math. Comput. Simulat., 72 (2006), 237.

[24] S. S. Chikatamarla, S. Ansumali and I. V. Karlin, Entropic lattice Boltzmann models for hydrodynamics in three dimensions, Phys. Rev. Lett., 97 (2006), 010201.

[25] S. S. Chikatamarla, S. Ansumali and I. V. Karlin, Grad's approximation for missing data in lattice Boltzmann simulations, Europhys. Lett., 74 (2006), 215.

[26] B. Alexeev, Generalized Boltzmann Physical Kinetics, Elsevier, 2004.

[27] Y. Peng, C. Shu and Y. T. Chew, Three-dimensional lattice kinetic scheme and its application to simulate incompressible viscous thermal flows, Commun. Comput. Phys., 2 (2007), 239.